DEPARTMENT OF MATERIALS SCIENCE & ENGINEERING
LEHIGH UNIVERSITY
John N. DuPont, PhD, FASM, FAWS
R.D. Stout Distinguished Professor, Materials Science & Engineering Department
Associate Director, Energy Research Center
Site Director, NSF Center on Integrated Materials Joining Science for Energy Applications
5 East Packer Avenue
Bethlehem, PA 18015-3195
Phone (610) 758-3942
FAX (610) 758-4244
e-mail jnd1@lehigh.edu

July 31, 2017

To Whom it May Concern:

Please find enclosed the Final Technical Report for Office of Naval Research Grant No. N00014-12-1-0475. Please do not hesitate to contact me directly if you need any additional information.

Regards,

John N DuPont

John N. DuPont, PhD, FASM, FAWS
R.D. Stout Distinguished Professor, Materials Science & Engineering Department
Associate Director, Energy Research Center
Site Director, NSF Center on Integrated Materials Joining Science for Energy Applications

REPORT DOCUMENTATION PAGE

Form Approved
OMB No. 0704-0188

1. REPORT DATE *(DD-MM-YYYY)*	2. REPORT TYPE	3. DATES COVERED *(From - To)*
31-07-2017	Final Report	01-06-2012 to 31-05-2016

4. TITLE AND SUBTITLE
Fundamental Studies on Phase Transformations and Mechanical Properties of Fusion Welds in Advanced Naval Steels

5a. CONTRACT NUMBER

5b. GRANT NUMBER
N00014-12-1-0475

5c. PROGRAM ELEMENT NUMBER

6. AUTHOR(S)
DuPont, John, N.

5d. PROJECT NUMBER

5e. TASK NUMBER

5f. WORK UNIT NUMBER

7. PERFORMING ORGANIZATION NAME(S) AND ADDRESS(ES)
Lehigh University, Department of Materials Science and Engineering
5 East Packer Avenue
Bethlehem, PA 18015

8. PERFORMING ORGANIZATION REPORT NUMBER
31-07-2017

9. SPONSORING/MONITORING AGENCY NAME(S) AND ADDRESS(ES)
Office of Naval Research
230 South Dearborn
Room 380
Chicago, IL 60604 - 1595

10. SPONSOR/MONITOR'S ACRONYM(S)
ONR

11. SPONSOR/MONITOR'S REPORT NUMBER(S)

12. DISTRIBUTION/AVAILABILITY STATEMENT
Approved for Public Release; distribution is unlimited

13. SUPPLEMENTARY NOTES

14. ABSTRACT
NUCu-140 and 10 wt% Ni steel were developed as candidate materials for use in naval and structural applications. However, prior to this research project, a fundamental understanding of the phase transformation behavior under the high heating and cooling rates associated with welding thermal cycles was not available for these alloys. For NUCu-140, the potential use of multiple thermal cycles was investigated with HAZ simulations using a Gleeble thermo-mechanical simulator. For 10 wt% Ni steel, the effect of rapid heating and cooling rates associated with welding thermal cycles was established for the first time.

15. SUBJECT TERMS
Welding, NUCu-140 Steel, 10 wt% Ni Steel, Phase Transformations

16. SECURITY CLASSIFICATION OF:			17. LIMITATION OF ABSTRACT	18. NUMBER OF PAGES	19a. NAME OF RESPONSIBLE PERSON
a. REPORT	b. ABSTRACT	c. THIS PAGE			John DuPont
					19b. TELEPHONE NUMBER *(Include area code)*
U	U	U	UU	19	610-758-3942

Fundamental Studies on Phase Transformations and Mechanical Properties of Fusion Welds in Advanced Naval Steels

Final Technical Report
ONR Grant Number N00014-12-1-0475

Lehigh University
Department of Materials Science and Engineering
Bethlehem, PA 18015

Technical Contact:
Prof. John N. DuPont, Principal Investigator
Department of Materials Science and Engineering
5 East Packer Avenue
Bethlehem, PA 18015
(610) 758-3942
jnd1@lehigh.edu

Abstract

Many US Naval applications exist that require the use of steels with high strength and resistance to fracture at low temperatures. NUCu-140 and 10 wt% Ni steel were developed as candidate materials for use in naval and structural applications. However, prior to this research project, a fundamental understanding of the phase transformation behavior under the high heating and cooling rates associated with welding thermal cycles was not available for these alloys. For NUCu-140, the potential use of multiple thermal cycles was investigated with HAZ simulations using a Gleeble thermo-mechanical simulator. Microhardness measurements revealed no strength recovery in the multipass HAZ samples. The time dependent precipitate characteristics were modeled under the HAZ thermal cycle conditions, and the results showed that the lack of strength recovery could be attributed to insufficient time for re-precipitation during the secondary weld pass. Conversely, full strength recovery in the HAZ was observed in the isothermally heat treated GTAW samples. Atom-probe tomography (APT) analysis correlated this strength recovery to re-precipitation of the copper-rich precipitates during the isothermal PWHT. For 10 wt% Ni steel, the effects of rapid heating and cooling rates associated with welding thermal cycles on the phase transformations and microstructures were determined. Heating rate experiments demonstrate that the Ac_3 temperature is dependent on heating rate, varying from 848°C at a heating rate of 1°C/s to 1051°C at a heating rate of 1830°C/s. A continuous cooling transformation diagram produced for 10 wt% Ni steel reveals that martensite will form over a very wide range of cooling rates, which reflects a very high hardenability of this alloy. These results were applied to a single pass GTAW. The diffusion of nickel from regions of austenite to martensite during the welding thermal cycle manifests itself in a muddled, rod-like lath martensitic microstructure. Additionally, with increasing peak temperature of the thermal cycle, the volume fraction of austenite decreases because of the destabilization of the austenite, brought on by the diffusion of Ni into the martensite regions. The results of these studies show that the nickel enrichment of the austenite in 10 wt% Ni

steel plays a critical role in phase transformations during welding. The findings of this research study provides a scientific basis for eventual full-scale use of these alloys in welded construction for naval applications.

Research on Cu-Bearing Steels

Research at Northwestern University has led to the development of a copper enriched precipitation strengthened steel (NUCu-140) that provides several significant advantages relative to currently used steels in terms of mechanical properties, cost, reduction of toxic welding fumes, and weldability[1–7]. This steel can exhibit a yield strength of 150 ksi, an impact energy of 150 ft-lbs at room temperature, and 20% elongation to failure. The attractive mechanical properties have been achieved with significant cost reduction through minimization of expensive alloying elements (e.g. Mo, Cr, and V) and use of simple and inexpensive processing techniques. The use of NUCu steel as a replacement for conventional structural plate material permits material and fabrication cost savings approaching 20% - 35%. Furthermore, these steels do not contain Cr, which eliminates the safety hazards associated with the formation of toxic hexavalent chromium in the welding fume[8].

Replacement of currently utilized materials with NUCu-140 cannot proceed without a thorough understanding of the welding response under a wide range of processing conditions. This knowledge was established in early research sponsored by the Office of Naval Research that involved collaboration between Lehigh University and Northwestern University[9–12]. Since NUCu-140 is a precipitation strengthened material, a detailed understanding is needed of the precipitate evolution that occurs in the heat-affected zone (HAZ) as a result of welding thermal cycles. A combination of dilatometry, HAZ simulations, LEAP tomography, modeling, and *in-situ* mechanical testing was used understand the microstructure and mechanical properties that develop in the HAZ of NUCu-140. LEAP tomography results demonstrated that local softening occurs as a result of dissolution of the Cu-rich precipitates. MatCalc kinetic simulations and strengthening calculations were conducted to model the observed precipitate and mechanical property trends. The microhardness and tensile testing results demonstrated local softening in the HAZ of NUCu-140 welds. The MatCalc simulations showed that a combination of partial dissolution, full dissolution, and re-precipitation of the Cu-rich precipitates occurs in the various HAZ regions. The predicted precipitate parameters were used as input to the Russell-Brown strengthening model to reveal the expected reductions in strength due to changes in precipitate features. The measured and predicted strength levels exhibited good very quantitative agreement for low heat input welding simulations.

As part of this ONR Grant, these fundamental research results were extended to identify simplified processing methods for restoring the loss in HAZ strength[13]. This research took advantage of the unique HAZ microstructure of this steel in which the precipitates exhibited dissolution, but no coarsened region. This is highly unusual, as nearly all precipitation strengthened materials form both a precipitate dissolution and coarsened region in the HAZ[14,15]. The presence of both the dissolution and coarsened regions necessitates a solution-quench-age post weld heat treatment to fully restore the HAZ mechanical properties. Such a treatment is expensive, time consuming, and cannot be practically applied to large structures. However, the absence of the coarsened region in the HAZ of NUCu-140 provided the potential for developing a direct, low

temperature age treatment without the need for the high temperature solution and quench steps of the process. Successful development of such a simple treatment would have significant benefits as it would help ensure full scale use of this alloy on the type of large structures of interest to the US Navy. In this research two possible treatment routes were explored – controlled multiple thermal cycles and direct aging. The research was fully supported by sophisticated modeling and microstructural characterization to develop fundamental knowledge of phase transformations and associated properties.

With the controlled multiple thermal cycle approach, the lower temperature thermal cycle of a secondary weld pass was used in attempt to promote re-precipitation in the HAZ of the previous weld pass. Welding with the use of multiple weld passes is common practice in the joining of thick plates in naval applications. Figure 1 shows the Vickers microhardness measurements of multi-pass HAZ simulated samples with a heat input of 0.75 kJ/mm. Each set of columns represents an initial peak temperature while each column within the grouping represents a subsequent secondary peak temperature or the as-welded condition. The base metal is represented by the single column. These results show no statistical improvement in microhardness between the as-welded (only initial peak temperature) and multi-pass weld HAZ for the 0.75 kJ/mm heat input samples. Similar results were observed for the 1.5 kJ/mm heat input experiments. The higher hardness in the coarse grain HAZ (CGHAZ) region as compared to the fine grain HAZ (FGHAZ) is not due to any re-precipitation of Cu precipitates but is due to the formation of an acicular ferritic microstructure and its fine substructure[9,10]. To better understand the microhardness results, the evolution of the Cu-rich precipitates during the weld thermal cycles was modeled using the MatCalc modeling code. The compositional dependence of interfacial energy and chemical driving force are taken into account in MatCalc, which provides a significant improvement over the classical nucleation, growth, and coarsening models when applied to the Fe-Cu system. The modeling was conducted in two steps, where the initial base metal heat treatment was first simulated, followed by the multi-pass weld HAZ thermal cycle. Precipitation modeling results for the 0.75 heat input simulation are summarized in Figure 2. The results for the as welded condition are plotted using a secondary peak temperature of 540°C for graphical purposes. It can be seen from these results that there is no significant change in the precipitate phase fraction between the single and multi-pass weld simulations for any combination of peak temperatures except for an initial peak temperature of 1350°C, for which there is an increase in phase fraction after a second weld thermal cycle. This demonstrates that there is insufficient time during the weld thermal cycle for precipitate nucleation and growth.

Figure 3 shows more promising results associated with the direct aging heat treatment. In this phase of the research, single pass Gas Tungsten Arc Welds (GTAW) were prepared on NUCu-140 and used for direct age treatments at various times. Figure 3 shows the microhardness traces across all regions of the weld in the as-welded condition compared to that after aging at 500°C for various times. For all aging times, the samples display an increase in hardness in the HAZ and FZ to levels higher than that of the base metal and as-welded HAZ. The hardness in the HAZ generally increases with aging time from one to ten hours, with only a slight change from 10 to 16 hours. The increase in hardness with aging time is most notable in the lower temperature region of the HAZ. Also, it can be seen that there is no decrease in the base metal hardness after aging at 500°C

for up to 16 hours. These observations are significant because they indicate that aging at 500°C for one hour, or even possibly less time, is adequate for increasing the hardness of the HAZ and fusion zone (FZ) without incurring any loss of hardness in the base metal. Similar results were obtained for a direct age temperature of 550°C.

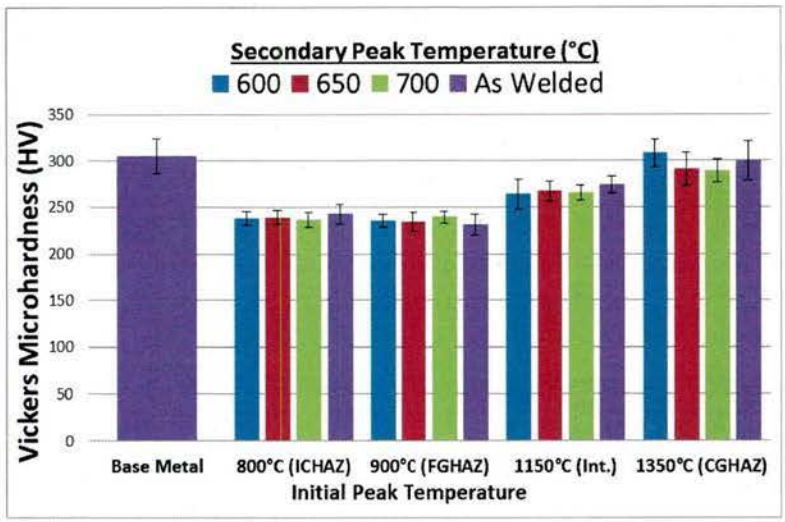

Figure 1. Vickers microhardness of base metal and simulated weld HAZs in NUCu-140 using an initial and secondary peak temperature for a heat input of 0.75 kJ/mm.

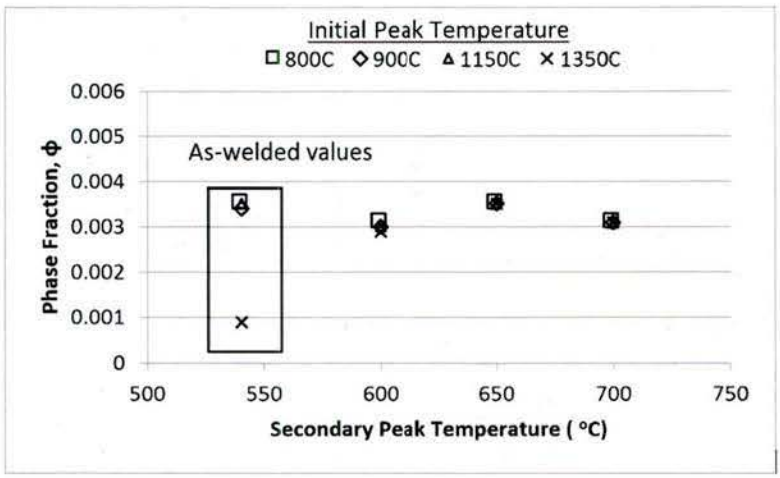

Figure 2. Summary of MatCalc simulation results showing the change in phase fraction of Cu-precipitates in NUCu-140 steel as a function of initial and secondary peak temperature for a heat input of 0.75kJ/mm.

LEAP tomography was utilized to study the evolution of Cu precipitates in the HAZ, FZ and base metal regions of the GTA welded sample and in the directly-aged sample and key results are shown in Figure 4. The Cu precipitates were not detected in the HAZ (Figure 4b) and FZ (Figure 4c) regions of the as welded sample. Re-precipitation of the Cu-precipitates occurred in the FZ (Figure 4d) and the HAZ (Figure 4e) regions in the directly-aged sample. The composition of the Cu-rich precipitates, their interfaces, and the surrounding matrix was measured and is shown

in Figure 5, which show enrichment of Ni, Al, and Mn at the precipitate/matrix interface and the precipitate core. Local enrichment of these elements lowers the interfacial energy and hence the coarsening rate of the Cu precipitates. The interfacial segregation also leads to the formation of an ordered B2-Ni (Al, Mn) phase at the matrix/precipitate interface[16] that serves as an effective barrier to Cu diffusion. In the present study, the softening that occurred in the HAZ and FZ of the as-welded sample was due to the dissolution of Cu precipitates and not due to their coarsening in these regions. The dissolution of Cu precipitates in the HAZ and FZ of the as-welded sample and the unaffected BM strength during PWHT at 500°C allows use of a simple direct aging isothermal treatment to re-precipitate Cu precipitates in these zones, thus avoiding the solution-quench-age process typically required of other precipitation hardened alloys after welding.

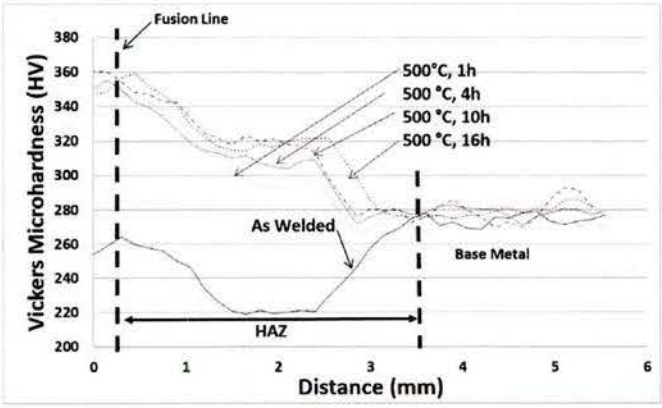

Figure 3. Microhardness traverses for the as-welded NUCu-140 GTA weld sample and for the NUCu-140 GTA weld sample aged at 500°C for various aging times.

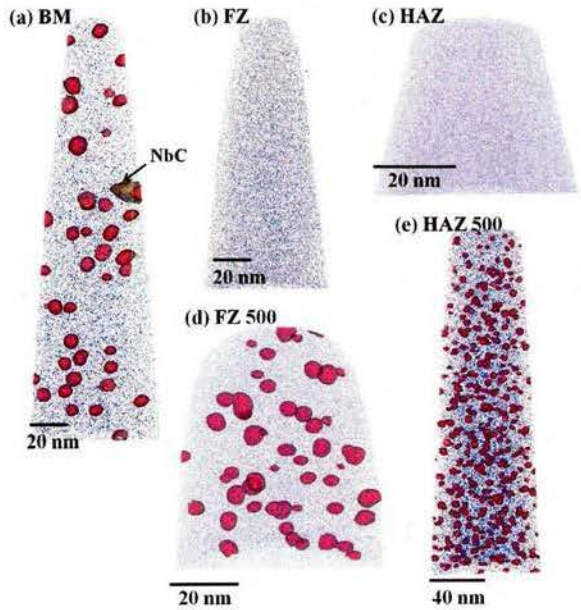

Figure 4. 3-D APT reconstructions of the samples that represent (a) BM, (b) FZ, (c) HAZ, (d) FZ 500, and (e) HAZ 500 regions. Cu precipitates are delineated by Cu-10 at.% isoconcentration surfaces (shown in red).

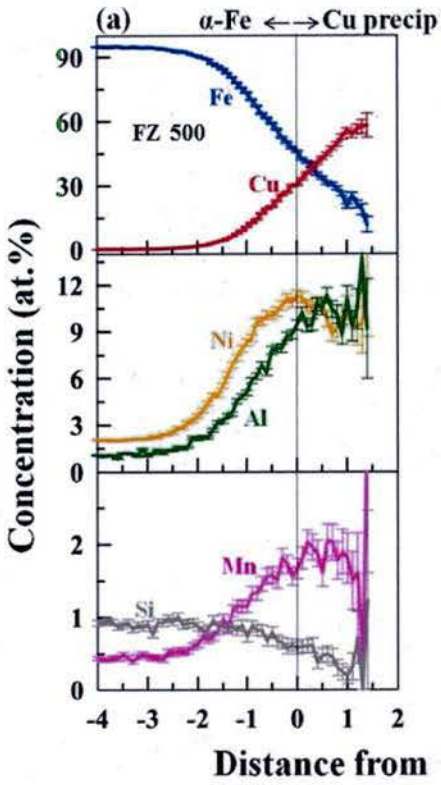

Figure 5. Proximity histogram concentration profiles of Fe, Cu, Ni, Al, Mn and Si across the α-Fe/Cu precipitate interface, obtained from the Cu precipitates in the FZ 500 regions of the NUCu-140 GTA weld sample that was directly aged for 10 hours at 500°C.

MatCalc modeling of the Cu precipitates was done for every combination of peak temperature, aging temperature, and aging time to gain a basic understanding of the precipitation kinetics. A summary of the predicted evolution of Cu precipitate phase fraction for each of the simulated HAZ regions during the PWHT at 500 is displayed in Figure 6. Results are shown for the various peak temperatures of interest as noted on the figures – 800, 900, 1150, and 1350°C. Results for the base metal are also shown for comparison. The phase fraction reaches its maximum of one volume percent after aging for one hour at 500°C. This is in agreement with the hardness measurements. The simulations for samples aged at 550°C show similar trends.

These results carry significant scientific and practical implications as they demonstrate that: 1) local segregation of select elements to the matrix/precipitate interface can be used to eliminate coarsening during the weld thermal cycle and 2) as a result, the mechanical properties can be restored with a simple low temperature direct age treatment. This represents the first study of its kind to demonstrate in detail that segregation can be used to eliminate precipitate coarsening in the HAZ, and also provides knowledge into the reason for eliminating the coarsening. Application of this knowledge to develop low temperature PWHT processes will help ensure this alloy can be utilized for large structures of interest to the US Navy.

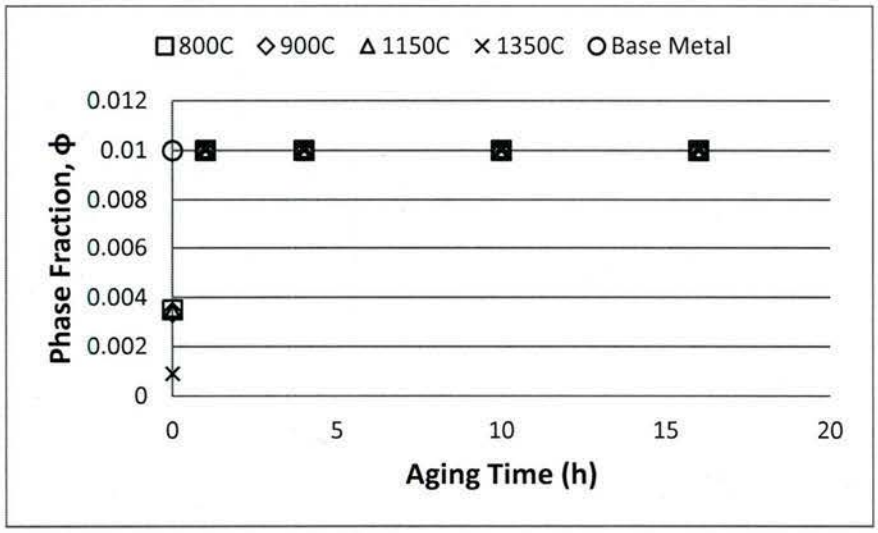

Figure 6. Summary of MatCalc simulation results showing variation in phase fraction of Cu-precipitates in NUCu-140 steel in BM and various HAZs as a function of aging time during isothermal PWHT at 500°C.

Research on 10 wt% Ni Steel

10 wt% Ni steel was developed to be used in naval applications, therefore both the strength and toughness of the steel is important. While it has already been proven that the steel has excellent strength and toughness[17,18], the effect of welding on these properties was not known at the beginning of the research project. The first part of the project studied the effects of heating and cooling rates on phase transformations in the steel, and their application to gas tungsten arc welding. Heating rate experiments were performed at two heating rates: 1°C/s and 1830°C/s to two peak temperatures, 1000°C and 1250°C. Figure 7 presents the curves of dilation as a function of temperature and their corresponding derivative for the heating rate experiments performed. Figures 7A and 7C show the curves for a slow heating rate of 1°C/s to peak temperatures of 1273 K (1000°C) and 1523 K (1250°C), respectively, while Figures 7B and 7D show the curves for a rapid heating rate of 1830°C/s to peak temperatures of 1273 K (1000°C) and 1523 K (1250°C), respectively. The critical temperatures Ac_1 (the temperature where austenite begins to form) and Ac_3 (the temperature where the sample has completely transformed to austenite), are indicated on the figure. The dilatometry plots in Figure 7 show that for the sample heated to a peak temperature of 1273 K (1000°C), at a 1°C/s heating rate, the Ac_1 temperature is 783 K (510°C) and the Ac_3 temperature is 1115 K (842°C), whereas at an 1830°C/s heating rate, the Ac_1 temperature is 861 K (588°C) and no Ac_3 temperature is observed. The evidence in Figure 3B that there is no Ac_3 temperature is that the slope of the derivative of the dilation never returns to zero, as the curve continues to be negative even after the large deviation in slope. For the samples heated to a peak temperature of 1523 K (1250°C), at a 1°C/s heating rate, the Ac_1 temperature is 836 K (563°C) and the Ac_3 temperature is 1121 K (848°C), whereas at an 1830°C/s heating rate, the Ac_1 temperature is 864 K (591°C) and the Ac_3 temperature is 1324 K (1051°C). These results show that the Ac_3 temperature has a strong dependence on heating rate. These results are significant for welding because the large temperature range between the Ac_1 and Ac_3 temperatures at high heating

rates will produce a large ICHAZ region. This is an important consideration when interpreting the HAZ microstructures. The experiments performed to determine the effects of cooling rate have shown that unlike current naval steels, the phase transformation behavior in 10 wt% Ni steel is highly insensitive to the cooling rate. Figure 8 shows this in the form of a Continuous Cooling Transformation (CCT) diagram that was recently developed through dilatometry measurements conducted on a Gleeble. This diagram shows that the M_s and M_f temperatures are relatively constant across all the cooling rates. The M_s temperature is 685 ± 38 K (412°C) and the M_f temperature is 466 ± 8 K (193°C). Furthermore, this CCT diagram is significant because it shows that martensite will form over a very wide range of cooling rates, which reflects a very high hardenability of 10 wt% Ni steel.

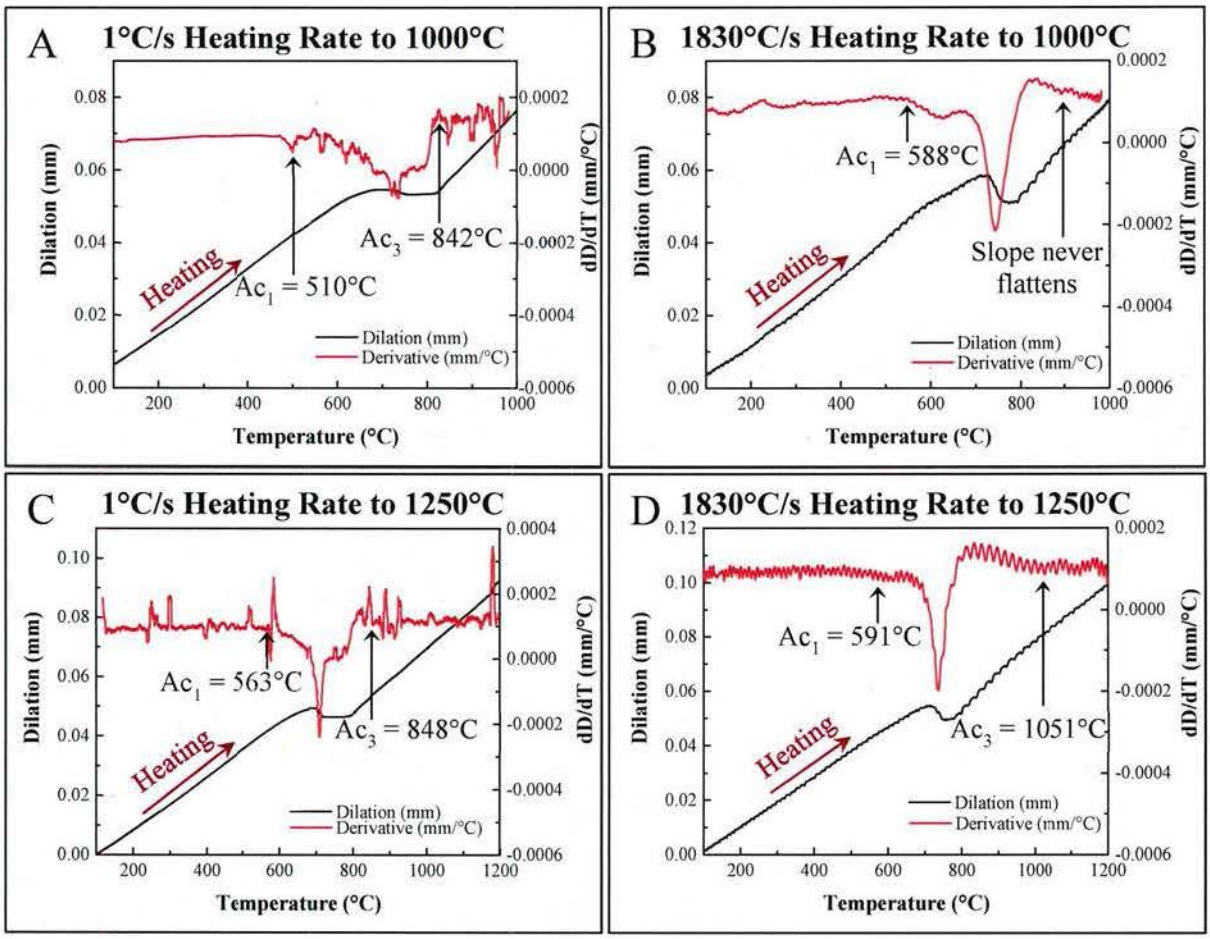

Figure 7. Dilatometry (black lines) and differentiated dilatometry (red lines) for the heating rate experiments. (A) and (B) were heated to a peak temperature of 1273 K (1000°C), while (C) and (D) were heated to a peak temperature of 1523 K (1250°C). Austenite start (Ac_1) and finish (Ac_3) temperatures are labelled accordingly.

Figure 9 shows a microhardness trace made across the cross-section of an autogenous, GTAW on QLT 10 wt% Ni steel weld. The results show that the hardness peaks at some finite distance from the fusion line, and the hardness in any region of the HAZ is never below the base metal hardness. Based on the microhardness results, select regions were chosen for

characterization and these regions, labelled A through F, are indicated on the microhardness trace in Figure 9. Figure 10 shows a scanning electron microscopy (SEM) micrograph of the base metal, to serve as a comparison. The base metal matrix consists of tempered lath martensite, which has a rod-like morphology. The rod-like light etching regions are consist of martensite + austenite, and appear lighter because of the high nickel content. There is also a coarse martensite constituent, indicated with arrows, and this constituent has been observed in similar 9 wt% and HSLA steels[19–21]. Figure 11 shows SEM micrographs of the various HAZ regions chosen for analysis. Using these micrographs, the microstructural evolution through the HAZ can be summarized as follows: Within the HAZ closest to the base metal, the appearance of the coarse martensite is different as some internal structure within the coarse martensite is seen in Figure 11A (indicated with arrows). The higher hardness of region A compared to the base metal suggests that some transformation on heating has occurred with as-quenched martensite forming on cooling. With further distance from the unaffected base metal, the coarse martensite disappears, first observed in Figure 11B. The disappearance of the coarse martensite is coincident with larger regions that appear to have transformed, which is circled in Figure 11B. At the highest hardness region, which is Figure 11C, the microstructure is a mixture of as-quenched lath martensite and rod lath martensite. With decreasing distance to the fusion line, the fraction of as-quenched lath martensite increases while the fraction of rod lath structure decreases. Figure 11E shows that the rod lath structure becomes increasingly muddled. Eventually, the rod structure is completely replaced by as-quenched lath martensite, which occurs beside the fusion zone. The microstructure next to the fusion zone in Figure 11F is a mixture of as-quenched lath martensite and coarse martensite.

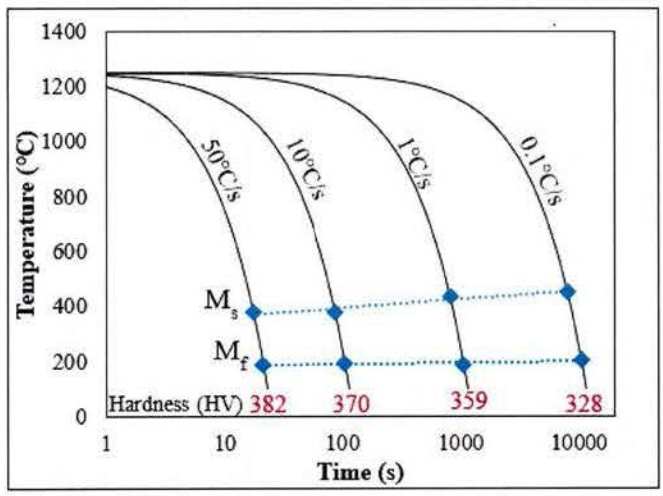

Figure 8. Continuous cooling transformation diagram for 10 wt% Ni steel.

Local electrode atom probe (LEAP) tomography was performed at Northwestern University on the base metal, region B, and region C. Figure 12 shows the 3D-reconstructions of the 3 regions. The base metal and region B both show M_2C carbides, whereas there are no carbides in region C. The compositions of the martensite and austenite were extracted from these reconstructions and are presented in Table 1. The concentration of Ni in the Ni-enriched region is lowest in Region C, intermediate in Region B, and highest in the base metal, whereas in the

martensite, the concentration of Ni is highest in Region C, intermediate in Region B, and lowest in the base metal. This suggests that during heating, the Ni is diffusing across the martensite/austenite interface from the high Ni regions to the martensite. A likely consequence of the lack of carbides in region C is that the carbon concentration in the austenite is higher than region B and the base metal, suggesting that carbides may have dissolved in this region.

It was mentioned that the rod lath structure becomes muddled with increasing distance from the fusion zone. This was also observed in the heating rate experiments. Figure 13 shows the microstructure of the heating rate sample that was heated at 1°C/s to a peak temperature of 1000°C. Based on the dilatometry results in Figure 7, this sample undergoes a complete transformation to austenite during heating, and during cooling this austenite transforms completely to as-quenched martensite. However, there is a subtle difference in the microstructure. There are two highlighted regions in Figure 13, labelled 1 and 2. Comparing the two areas, region 1 has dark contrast reminiscent of the rod lath structure whereas region 2 does not. This remnant rod structure would suggest that the sample did not fully transform to austenite during heating, but the dilatometry curves confirm that this sample did completely transform. As was described for the base metal, the light etching, rod features are regions of martensite + austenite, and the light etching is an effect of the high Ni concentration of these regions. Also, it is known that Ni is diffusing across the martensite/austenite interface during welding. Since Ni diffusion in Fe is one of the slowest diffusing elements, there is not enough time during heating for the Ni to completely homogenize, so the residual rod lath microstructure is still observed because of the remnant compositional differences. This is unusual and has not previously been observed in quenched and tempered steels. This makes it difficult to distinguish microstructures in the HAZ of 10 wt% Ni steel that were heated to above the Ac_3 temperature from those that were heated to intermediate temperatures between Ac_1 and Ac_3.

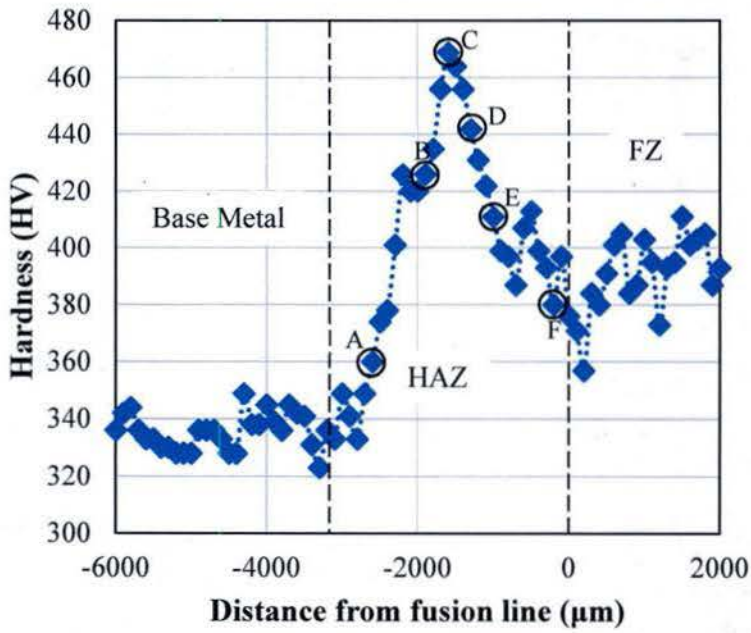

Figure 9. Microhardness trace across the gas tungsten arc weld that was made on 10 wt% Ni steel base plate. Circled indents are regions used for analysis.

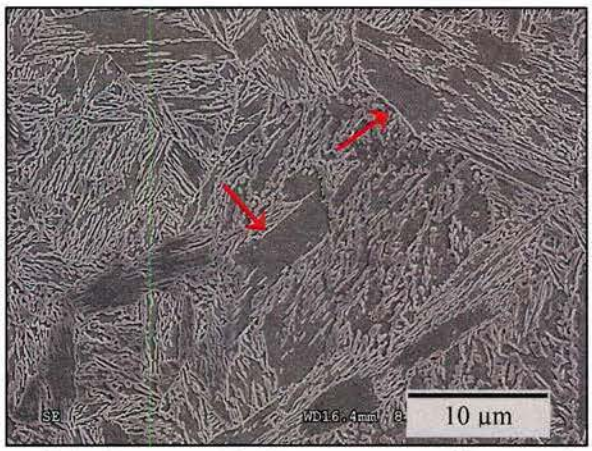

Figure 10. Microstructure of the base metal. Coarse martensite constituent indicated by arrows.

Having established the phase transformations that occur with heating and cooling in 10 wt% Ni steel, the mechanical properties were evaluated in the HAZ. Samples were prepared in a Gleeble 3500 thermo-mechanical simulator using thermal cycles generated by Sandia's Smartweld program[22] for a range of peak temperatures that would be experienced in an actual weld. Eight peak temperatures were chosen to match microstructures exhibited in the GTAW, and the simulated thermal cycles for these peak temperatures are shown in Figure 14. The designations of the regions of the HAZ in Figure 14 are based on the heating rate experiments in Figure 7. Figure 15 shows how the retained austenite content, impact toughness at room temperature, and yield strength each vary as a function of the peak temperature within the HAZ. The yield strength results are shown in red, and they demonstrate that the highest strength is in the 825°C peak temperature sample, which is an ICHAZ sample. High strength is also observed in peak temperatures of 925, 1000, and 1150°C. The Charpy impact toughness is shown in black. The results show that there is low toughness in the peak temperature regions of 825, 925, and 1000°C. Since 10 wt% Ni steel is a TRIP-assisted steel, its toughness depends on the retained austenite content[17,18]. Therefore, the retained austenite content was evaluated for each peak temperature, and these results are shown in blue in Figure 15. There is a trend of decreasing retained austenite content with increasing peak temperature. The trend of decreasing retained austenite with increasing peak temperature was initially thought to be a concern for the toughness of these regions. The same trend of decreasing retained austenite content with increasing peak temperature was observed for similar 9 wt% Ni steels. In research by Nippes and Balaguer[23] and Jang *et al.*[24], the toughness of the HAZ was directly related to the retained austenite content, as a decrease in retained austenite produced a decrease in the toughness. For 10 wt% Ni steel, the toughness does decrease with decreasing retained austenite content only up through a peak temperature of 1000°C. For the peak temperature of 1150°C, the retained austenite content is 1.2 ± 0.7 vol%, but its toughness is 106 ± 6 ft-lbs, which in fact is nearly the same as the base metal values of 106 ± 2 ft-lbs. The toughness of the 1250 and 1350°C peak temperatures is also quite high at 85 ± 4 and 95 ± 3ft-lbs, respectively, with almost no detectable retained austenite. Therefore, the high impact toughness must be provided by a mechanism other than retained austenite. This idea that the retained austenite is not the only microstructural factor affecting toughness is further reinforced by comparing the impact toughness

of the peak temperatures 725 and 825°C. Both samples have similar retained austenite values, however, the toughness of 725°C at 99 ± 8 ft-lbs is nearly double 825°C at 54 ± 0 ft-lbs.

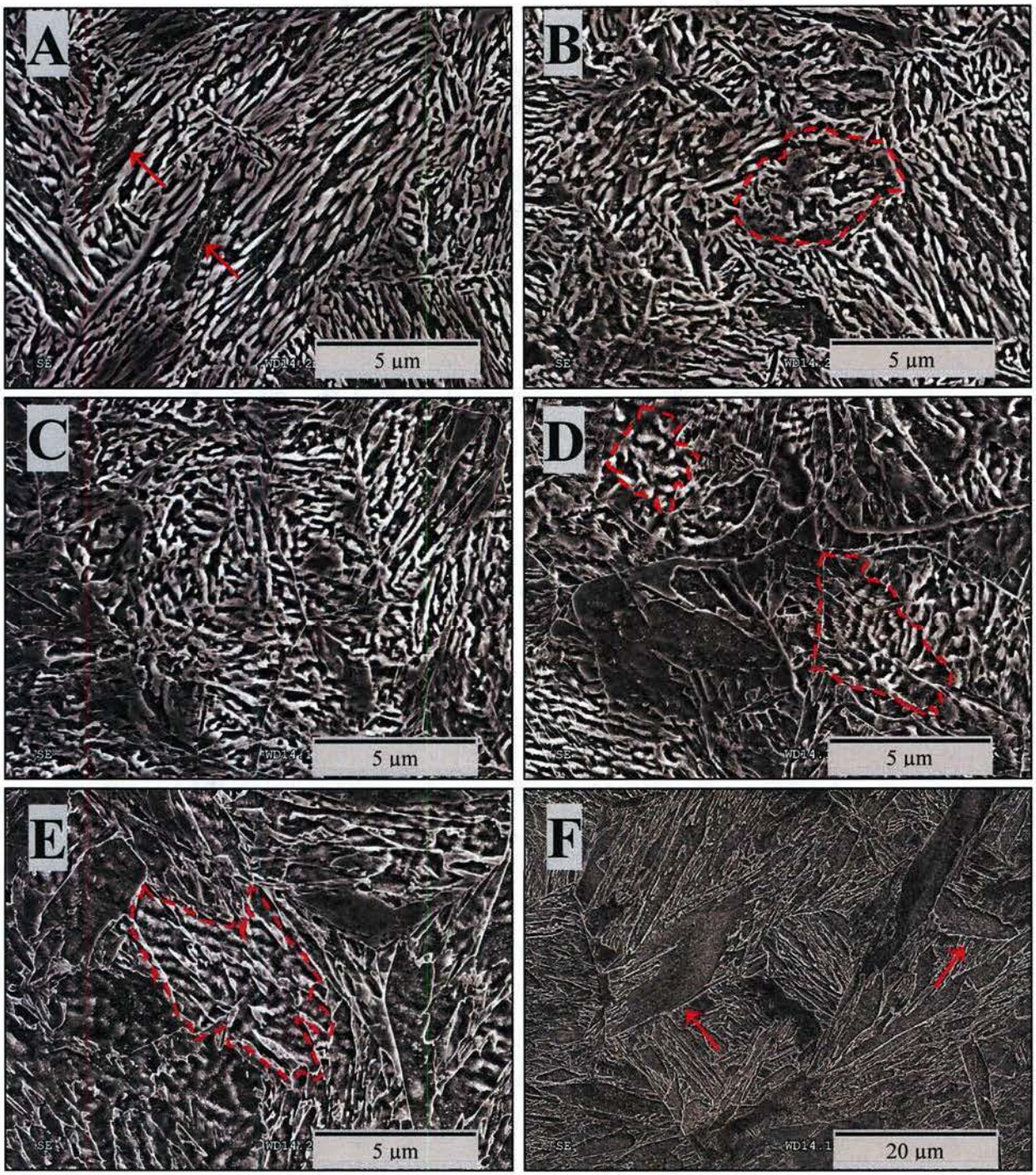

Figure 11. SEM micrographs of selected regions of the gas tungsten arc weld made on QLT heat treated base plate. The regions (A), (B), (C), (D), (E), and (F) correspond to the circled indents on the microhardness trace in Figure 9.

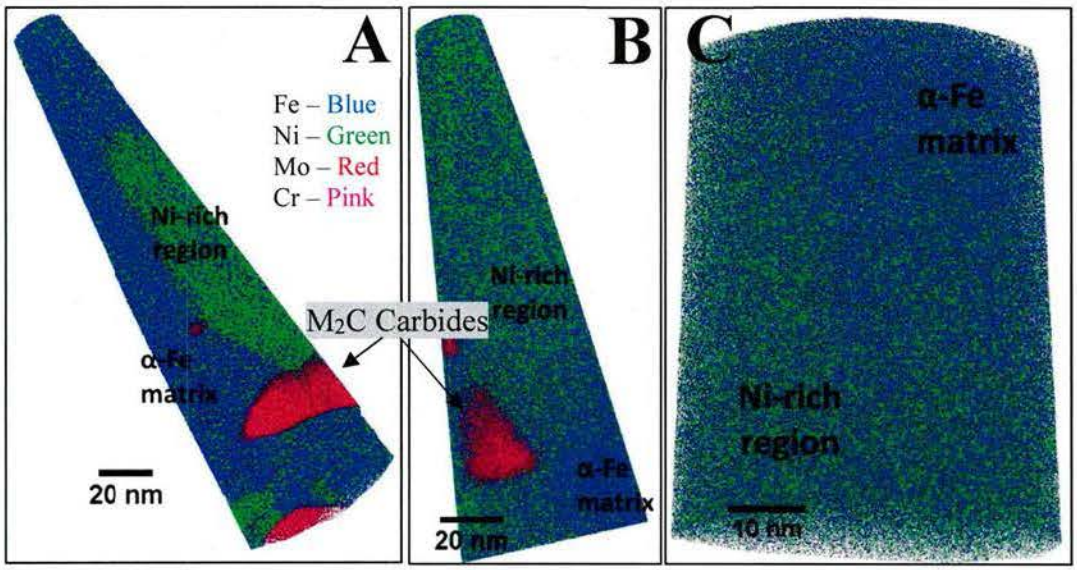

Figure 12. Local electrode atom probe tomography 3D reconstructions for the (A) base metal, (B) region B, and (C) region C. Fe atoms are in blue, Ni atoms are in green, Mo and Cr are in red and pink, respectively

Table 1. Composition of 10 wt% Ni steel. The nominal overall composition was measured by optical emissions spectroscopy. The compositions of martensite and austenite were measured using the LEAP tomography from Figure 12. All compositions are in wt%.

	Fe	C	Ni	Mo	V	Cr	Mn	Si	Cu
Nominal overall	87.50	0.47	9.22	0.90	0.07	0.70	0.65	0.36	0.14
Martensite (BM)	92.4 ± 0.12	0.08 ± 0.01	6.00 ± 0.10	0.24 ± 0.02	0.02 ± 0.006	0.54 ± 0.03	0.29 ± 0.02	0.32 ± 0.02	0.07 ± 0.01
Martensite (region B)	89.66 ± 0.52	0.07 ± 0.03	7.69 ± 0.46	0.39 ± 0.11	0.04 ± 0.03	0.65 ±0.14	0.62 ± 0.13	0.64 ± 0.13	0.12 ± 0.06
Martensite (region C)	88.24 ± 0.49	0.33 ± 0.09	8.71 ± 0.43	0.36 ± 0.09	0.05 ± 0.03	0.65 ± 0.12	0.88 ± 0.14	0.47 ± 0.10	0.12 ± 0.05
Austenite (BM)	77.73 ± 0.20	0.37 ± 0.03	18.26 ± 0.19	0.31 ± 0.03	0.02 ± 0.01	0.88 ± 0.05	1.64 ± 0.06	0.36 ± 0.03	0.29 ± 0.03
Austenite (region B)	80.05 ± 0.31	0.96 ± 0.07	15.51 ± 7.69	0.57 ± 0.06	0.09 ± 0.02	0.83 ± 0.07	1.13 ± 0.08	0.45 ± 0.05	0.21 ± 0.04
Austenite (region C)	80.03 ± 0.26	2.67 ± 0.11	13.78 ± 0.23	0.48 ± 0.04	0.07 ± 0.02	0.83 ± 0.06	1.17 ± 0.07	0.44 ± 0.04	0.23 ± 0.03

The LEAP results, though performed on the GTAW, are useful for interpretation of the mechanical property trends. As previously discussed, during the welding thermal cycle, the Ni diffuses from the austenite to the martensite. Since Ni is an austenite stabilizer[25], it is suggested

that the Ni diffusing out of the austenite is making the austenite less stable, so on cooling, the austenite transforms to martensite instead of being maintained as retained austenite. Thus, with increasing peak temperature, there is less retained austenite present at room temperature because the Ni has begun to homogenize across the microstructure. The LEAP results can also help to explain the low toughness and high strength of the ICHAZ. Region C in the GTAW is an ICHAZ region, and the reason for that was determined from the hardness of the simulated HAZ regions. The hardness of the SCHAZ, which was heated to a peak temperature of 550°C is 331 ± 5 HV. From the hardness plot in Figure 9, the hardness of the base metal is 335 ± 6 HV. This shows that there is no statistical difference in the hardness of the base metal or the SCHAZ. Since the hardness of region A in the GTAW is 360 HV, which is harder than the base metal, this suggests that region A is the beginning of the ICHAZ. Therefore, regions A through D are part of the ICHAZ. As was previously described, no carbides were found in region C in the LEAP reconstructions. As shown in Table 1, the carbon content of the Ni-rich region in region C is 2.67 ± 0.11 at% which is much higher than any other region. This suggests that a carbide has dissolved in this region. Since the ICHAZ regions have half as much austenite as the base metal, some of that austenite is transforming to as-quenched martensite on cooling. Therefore, this high carbon austenite is transforming to martensite during cooling. The hardness of as-quenched martensite is directly proportional to the carbon content, so this high carbon martensite is likely very hard and can act as a local brittle zone[26]. Since carbon is a fast diffuser, at the higher peak temperatures there is more time for diffusion so the carbon can homogenously distribute over the microstructure, thereby eliminating the high carbon martensite, so the toughness is higher in the 1150°C, 1250°C, and 1350°C peak temperature samples. Therefore, the cause for the high strength and low toughness in the ICHAZ is local brittle zones caused by high carbon martensite. This is significant because it was previously thought that the retained austenite was the sole factor in determining the toughness of 10 wt% Ni steel. However, the ballistic resistance of the steel was not investigated in this study and the results for ballistic resistance and toughness can be very different, therefore, it is suggested that ballistic resistance studies be performed as a function of peak temperature as well.

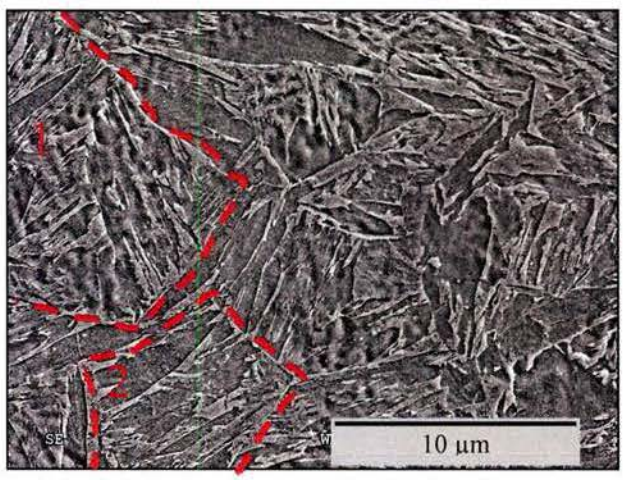

Figure 13. SEM micrograph of the samples used for the heating rate studies that was heated at 1°C/s to a peak temperature of 1000°C.

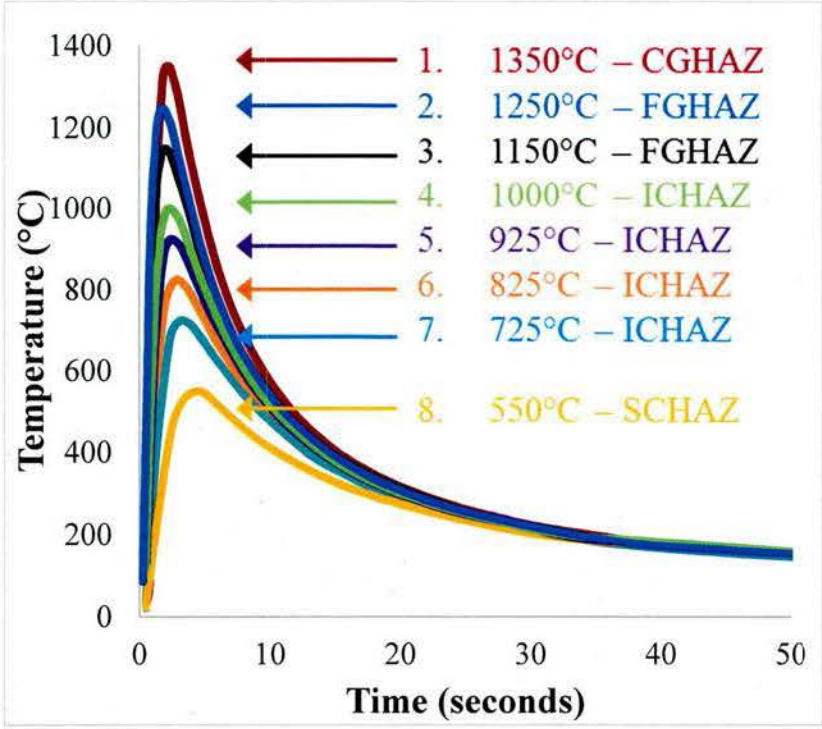

Figure 14. SmartWeld calculated thermal cycles for a heat input of 1500J/mm. The peak temperautre HAZ designations are based on the results of the heating rate study.

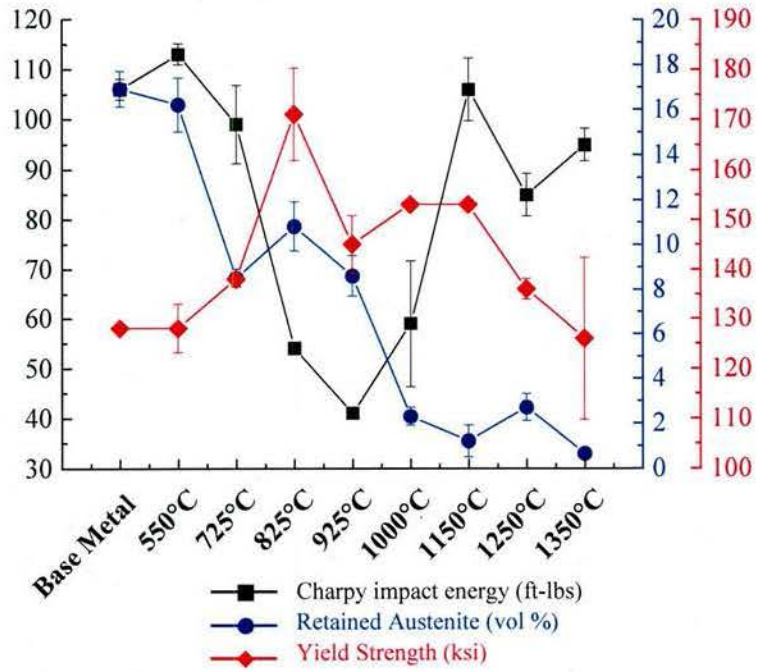

Figure 15. Variation in retained austenite, yield strength, and Charpy impact toughness in 10 wt% Ni steel as a function of peak temperature.

Conclusions

Recent ONR-sponsored research lead by Lehigh University (in collaboration with Northwestern University) has developed a fundamental understanding of phase transformations and mechanical properties in the HAZ of NUCu-140 steel and 10 wt% Ni steel. The following conclusions can be drawn from this work:

1. *NUCu-140:*
    a. Welds on NUCu-140 exhibit local softening in the fusion zone and heat-affected zone as a result of the fusion weld thermal cycle.
    b. Multipass weld simulations did not produce an increase in hardness of the heat-affected zone after a high initial peak temperature followed by a lower secondary peak temperature. MatCalc simulations indicate that the time is too short to promote significant re-precipitation of the Cu-rich precipitates during the secondary weld thermal cycle.
    c. Isothermal post-weld heat treatments of GTA welds at 773 and 823 K (500 and 550°C) demonstrated an increase in hardness of the fusion zone and heat-affected zone to levels above that of the base metal. Short aging times of 0.25 hour at 823 K (550°C) and 1 hour at 773 K (500°C) were adequate to increase the hardness of these zones to levels above that of the base metal.
    d. APT results and MatCalc simulations demonstrated that the softening in the heat-affected zone of the NUCu-140 weld is the result of the dissolution of the Cu-rich precipitates during the heating portion of the weld thermal cycle followed by little or no re-precipitation upon cooling. The dissolution of Cu precipitates in these zones combined with their negligible coarsening at aging temperature of 773 K (500°C) permits the use of a simple direct-aging treatment at 773 K (500°C) (without a prior solutionizing-quenching step) to recover the hardness in softened zones in NUCu140 without affecting the BM hardness.
2. *10 wt% Ni steel:*
    a. The Ac_1 and Ac_3 temperature of the steel are dependent on heating rate. The Ac_1 and Ac_3 temperatures when the sample is heated at 1°C/s are 836 K (563°C) and 1121 K (848°C), respectively, and the Ac_1 and Ac_3 temperatures when the sample is heated at 1830°C/s are 864 K (591°C) and 1324 K (1051°C), respectively.
    b. There is a large dependence on heating rate for the Ac_3 temperature. This is significant for welding because the large temperature range between the Ac_1 and Ac_3 temperatures at high heating rates will produce a large ICHAZ region. The mechanical property results demonstrate that this is the most concerning region of the HAZ because of the low toughness.
    c. The CCT diagram shows that martensite will form over a very wide range of cooling rates, which reflects a very high hardenability of 10 wt% Ni steel. The M_s temperature is 685 ± 38 K (412°C) and the M_f temperature is 466 ± 8 K (193°C).
    d. With increasing peak temperature of the thermal cycle, the volume fraction of retained austenite decreases. The LEAP tomography results suggest that this is due to the destabilization of the austenite brought on by the diffusion of Ni out of the austenite.

e. The toughness is lowest in the ICHAZ regions. The low toughness is a result of the dissolution of M_2C carbides during welding. When the carbides dissolve, they leave behind a region of high carbon content, which when cooled, transforms to brittle, as-quenched martensite.

Refereed Journal Articles

Jason T. Bono, John N. DuPont, Divya Jain, Sung-Il Baik, and David N. Seidman, Investigation of Strength Recovery in Welds of NUCu-140 Steel Through Multipass Welding and Isothermal Post-Weld Heat Treatments, *Metallurgical and Materials Transactions A,* 2015, Volume 46A, pp. 5727-5746.

Erin J. Barrick, Divya Jain, John N. DuPont, and David N. Seidman, Effects of Heating and Cooling Rates on Phase Transformations in 10 wt% Ni Steel and Their Application to Gas Tungsten Arc Welding, *Submitted to Metallurgical and Materials Transactions A*

Erin J. Barrick and John N. DuPont, Mechanical Properties and Microstructural Characterization of Simulated Heat Affected Zones in 10 wt% Ni steel, *In Preparation*

Presentations

Jason Bono and John DuPont, Welding of Advanced Naval Steels, FABTECH AWS Conference, November 20, 2013, Chicago, IL.

Jason Bono, Erin Barrick, John DuPont, Divya Jain, and David Seidman, Strength Recovery in NUCu-140 Through Multipass Weld Simulations and Isothermal Post-weld Heat Treatments, Materials Science and Technology, October 15, 2014, Pittsburgh, PA.

Erin Barrick and John DuPont, Phase Transformations and Mechanical Properties of Fusion Welds in 10 wt% Ni Steel, Materials Science and Technology, October 5, 2015, Columbus, OH.

Erin Barrick and John DuPont, Phase Transformations and Mechanical Properties of Fusion Welds in 10 wt% Ni Steel, FABTECH AWS Conference, November 12, 2015, Chicago, IL.

Erin Barrick and John DuPont, Phase Transformations and Mechanical Properties of the heat-affected zone in 10 wt% Ni Steel, Materials Science and Technology, October 26, 2016, Salt Lake City, UT.

Erin Barrick and John DuPont, Phase Transformations and Mechanical Properties of Fusion Welds in 10 wt% Ni Steel, FABTECH AWS Conference, November 16, 2016, Las Vegas, NV.

References

1. Isheim, D. & Seidman, D. N. Nanoscale studies of segregation at coherent heterophase interfaces in α-Fe based systems. *Surf. Interface Anal.* **36,** 569–574 (2004).

2. Isheim, D., Gagliano, M. S., Fine, M. E. & Seidman, D. N. Interfacial segregation at Cu-rich precipitates in a high-strength low-carbon steel studied on a sub-nanometer scale. *Acta Mater.* **54,** 841–849 (2006).
3. Kolli, R. P. & Seidman, D. N. Comparison of Compositional and Morphological Atom-Probe Tomography Analyses for a Multicomponent Fe-Cu Steel. *Microsc. Microanal.* **13,** 272–284 (2007).
4. Gagliano, M. S. & Fine, M. E. Characterization of the nucleation and growth behavior of copper precipitates in low-carbon steels. *Metall. Mater. Trans. A* **35,** 2323–2329 (2004).
5. Isheim, D., Kolli, R. P., Fine, M. E. & Seidman, D. N. An atom-probe tomographic study of the temporal evolution of the nanostructure of Fe–Cu based high-strength low-carbon steels. *Scr. Mater.* **55,** 35–40 (2006).
6. Prakash Kolli, R. & Seidman, D. N. The temporal evolution of the decomposition of a concentrated multicomponent Fe–Cu-based steel. *Acta Mater.* **56,** 2073–2088 (2008).
7. Prakash Kolli, R., Wojes, R. M., Zaucha, S. & Seidman, D. N. A subnanoscale study of the nucleation, growth, and coarsening kinetics of Cu-rich precipitates in a multicomponent Fe – Cu based steel. *Int. J. Mater. Res.* **99,** 513–527 (2008).
8. Castner, R. & Null, C. L. Chromium, Nickel, and Manganese in Shipyard Welding Fumes. *Weld. J.* 223s–231s (1998).
9. Farren, J. D., Hunter, A. H., Dupont, J. N., Seidman, D. N. & Robino, C. V. Microstructural evolution and mechanical properties of simulated heat affected zones in NUCu-140 steel. *Weld. J.* **92,** 140–s (2013).
10. Farren, J. D. *et al.* Microstructural Evolution and Mechanical Properties of Fusion Welds in an Iron-Copper-Based Multicomponent Steel. *Metall. Mater. Trans. A* **43,** 4155–4170 (2012).
11. Hunter, A. H., Farren, J. D., DuPont, J. N. & Seidman, D. N. An Atom-Probe Tomographic Study of Arc Welds in a Multi-Component High-Strength Low-Alloy Steel. *Metall. Mater. Trans. A* **44,** 1741–1759 (2013).
12. Hunter, A. H., Farren, J. D., Dupont, J. N. & Seidman, D. N. Multi-component Cu-strengthened steel welding simulations: Atom-probe tomography and synchrotron X-ray diffraction analyses. *Metall. Mater. Trans. A* **46A,** 3117–3131 (2015).
13. Bono, J. T., DuPont, J. N., Jain, D., Baik, S.-I. & Seidman, D. N. Investigation of Strength Recovery in Welds of NUCu-140 Steel Through Multipass Welding and Isothermal Post-Weld Heat Treatments. *Metall. Mater. Trans. A* **46,** 5158–5170 (2015).
14. Bhaduri, A. K. & Venkadesan, S. Microstructure of the heat-affected zone in 17–4 PH stainless steel. *Steel Res.* **60,** 509–513 (1989).
15. Rading, G. O., Shamsuzzoha, M. & Berry, J. T. A Model for HAZ Hardness Profiles in Al-Li-X Alloys: Applications to the Al-Li-Cu Alloy 2095. *Weld. J.* 411s–416s (1998).
16. Kolli, R. P., Mao, Z., Seidman, D. N. & Keane, D. T. Identification of a Ni0.5(Al0.5−xMnx) B2 phase at the heterophase interfaces of Cu-rich precipitates in an α-Fe matrix. *Appl. Phys. Lett.* **91,** 241903 (2007).
17. Isheim, D., Hunter, A. H., Zhang, X. J. & Seidman, D. N. Nanoscale Analyses of High-Nickel Concentration Martensitic High-Strength Steels. *Metall. Mater. Trans. A* **44,** 3046–3059 (2013).

18. Zhang, X. J. Microhardness characterisation in developing high strength, high toughness and superior ballistic resistance low carbon Ni steel. *Mater. Sci. Technol.* **28,** 818–822 (2012).
19. Fonda, R. W. & Spanos, G. Effects of Cooling Rate on Transformations in a Fe-9 Pct Ni Steel. *Metall. Mater. Trans. A* **45,** 5982–5989 (2014).
20. Fonda, R. W., Spanos, G. & Vandermeer, R. A. Observations of plate martensite in a low carbon steel. *Scr. Metall. Mater.* **31,** 683–688 (1994).
21. Spanos, G., Fonda, R. W., Vandermeer, R. A. & Matuszeski, A. Microstructural changes in HSLA-100 steel thermally cycled to simulate the heat-affected zone during welding. *Metall. Mater. Trans. A* **26,** 3277–3293 (1995).
22. Fuerschbach, P. W., Eisler, G. R. & Steele, R. J. Weld procedure development with OSLW - Optimization software for laser welding. in *Fifth International Conference on Trends in Welding Research* (1998).
23. Nippes, E. F. & Balaguer, J. P. A study of the weld heat-affected zone toughness of 9% nickel steel. *Weld. J.* **65,** 237s–243s (1986).
24. Jang, J., Yang, Y., Kim, W. & Kwon, D. Evaluation of cryogenic fracture toughness in SMA-welded 9% Ni steels through modified CTOD test. *Met. Mater.* **3,** 230–238 (1997).
25. H. K. D. H. Bhadeshia & R. W. K. Honeycombe. *Steels: Microstructure and Properties*. (Butterworth-Heinemann, 2006).
26. Krauss, G. *Steels: Processing, Structure, and Performance*. (ASM International, 2015).